Experimental Evaluation of Co-Manipulated Ultrasound-Guided Flexible Needle Steering

Momen Abayazid, Claudio Pacchierotti, Pedro Moreira, Ron Alterovitz, Domenico Prattichizzo, and Sarthak Misra

***Abstract*—*Background:* We present and evaluate a teleoperation system for bevel-tipped flexible needle steering. Robotic systems with autonomous control algorithms have been exploited as the main tool to achieve high accuracy and reliability. However for reasons of safety and acceptance by the surgical community, robotic control is not preferable.**

***Methods:* In our work, an ultrasound-guided control algorithm computes the optimal needle orientation during the insertion, but it does not directly control the needle's motion. Navigation cues about the computed optimal orientation are provided through a combination of haptic (vibratory) and visual feedback to the operator who controls the slave robot to steer the needle.**

***Results:* Four experimental conditions are conducted, enrolling subjects with a clinical background to study the targeting accuracy of different co-manipulation configurations.**

***Conclusions:* Experimental results show that receiving feedback from the control algorithm improves the targeting accuracy with a factor of 9 with respect to manual insertions.**

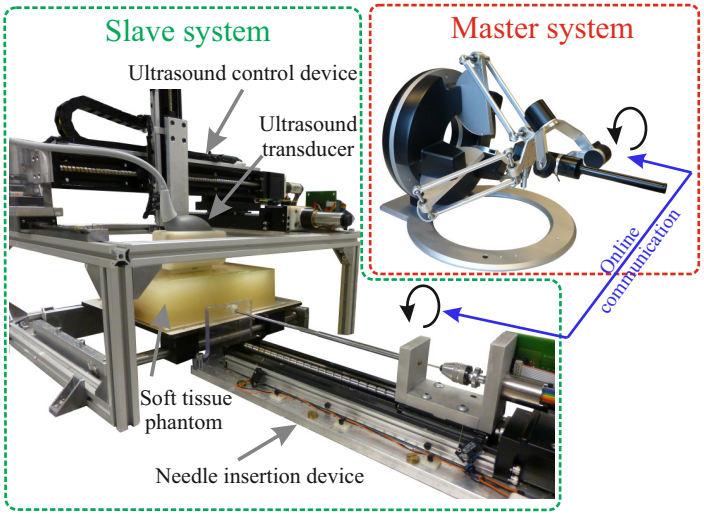

Fig. 1. The slave system represents the needle control device for needle insertion and rotation about its axis, and also the ultrasound control device used for three-dimensional needle tip tracking. The master device represents the haptic device that allows the operator to control the needle.

I. Introduction

Needle insertion into soft-tissue is a minimally invasive procedure used for diagnostic and therapeutic purposes. Examples of diagnostic needle insertion procedures are liver and lung biopsies to detect tumors [1]. Therapeutic applications of needle insertion include brachytherapy of cervical, prostate and breast cancers [2]. Imaging modalities such as ultrasound, magnetic resonance (MR), and computed tomography (CT) are often used during needle insertion procedures to accurately determine the needle and target positions [3]. Inaccurate placement of the needle may in fact result in misdiagnosis and unsuccessful treatment during biopsy and brachytherapy, respectively.

Flexible needles were introduced to provide enhanced steering capabilities, allowing the needle to avoid obstacles and accurately reach the target position [4]. Flexible needles fabricated with an asymmetric tip (e.g., bevel tip) naturally deflect during insertion into soft-tissue [5]. This can be exploited to make the needles move in non-straight paths and reach certain target position [4]. It is hypothesized that steering a needle with an asymmetric tip is not intuitive [4]. Control algorithms are required for accurate needle placement. These needles can be assumed to deflect along circular paths during insertion. This assumption is used in various studies to model the needle deflection during insertion [4], [5]. The deflection can be also controlled using duty-cycling of the needle during insertion [6]. This approach varies the needle curvature by changing the ratio between the period of needle insertion with spinning to the total period of insertion.

Several research groups have developed flexible needle deflection models for needle steering [4], [5]. Webster *et al.* showed that nonholonomic kinematics of the unicycle and bicycle models can be used to predict needle path during the insertion into soft tissue [5]. Hauser *et al.* developed a 3D feedback controller that steers the needle along a helical path, although results were evaluated only in simulation [7]. Furthermore, Abayazid *et al.* presented an autonomous two-dimensional (2D) ultrasound image-guided steering system, and a 3D robotic system where they used both Fiber Bragg Grating sensors and ultrasound for feedback [8]–[10].

In the aforementioned studies, the needle steering is performed autonomously and the operator does not intervene during insertion. The main advantage of autonomous robotic systems is providing a significantly higher accuracy with respect to that of manual insertions. However, autonomous systems are not currently widely accepted by the clinical

M. Abayazid, P. Moreira and S. Misra are affiliated with the Department of Biomechanical Engineering, MIRA - Institute for Biomedical Technology and Technical Medicine, University of Twente, Enschede, The Netherlands, S. Misra is also affiliated with the Department of Biomedical Engineering, University of Groningen and University Medical Centre, Groningen, The Netherlands. *(e-mail: {m.abayazid; p.lopesdafrotamoreira; s.misra}@utwente.nl).*

C. Pacchierotti and D. Prattichizzo are affiliated with the Department of Information Engineering and Mathematics, University of Siena, and with the Department of Advanced Robotics, Istituto Italiano di Tecnologia, Italy, *(e-mail: {pacchierotti; prattichizzo}@dii.unisi.it).*

R. Alterovitz is affiliated with the Department of Computer Science, University of North Carolina at Chapel Hill, USA, *(e-mail: ron@cs.unc.edu).*

community due to concerns about safety [11], [12]. For this reason, Hungr *et al.* developed an autonomous robotic system that switches to manual mode in case of predefined emergency conditions [13]. Majewicz and Okamura presented a teleoperated system where the operator commands the desired position in Cartesian space and the system provides force feedback that represents kinematic constraints and the position error of the robot. The evaluation of the system was based on simulations performed by an operator [14]. Finally, other researchers guarantee the insertion system safety using force feedback techniques [15], [16].

A. Haptic feedback for shared control

Robotic teleoperation systems enable operators to take control over the needle procedure, to guarantee the safety of the system, while achieving extreme accuracy and repeatability. Robotic teleoperation systems are composed of a slave robot, which interacts with a remote environment, and a master system, operated by a human (Fig. 1). The slave robot is in charge of resembling the movement of the operator who, in turn, needs to observe the environment the robot is interacting with. This is possible through different types of information that flow from the remote scenario to the operator. They are usually a combination of visual and haptic stimuli. Visual feedback is already employed in commercial robotic surgery systems (e.g., the da Vinci Si Surgical System, Intuitive Surgical, Sunnyvale, CA, USA) while it is not common to find commercially-available devices implementing haptic force feedback. One of the few examples is the Sensei robotic catheter system (Hansen Medical, Mountain View, CA, USA).

However, haptic feedback is widely considered to be a valuable navigation tool during teleoperated surgical procedures [14], [17]. It enhances clinicians' performance in terms of completion time of a given task [18], accuracy [19], peak and mean applied force [17], [18], [20]. In medicine, haptic feedback has been shown to improve performance in fine microneedle positioning [21], telerobotic catheter insertion [22], suturing simulation [23], cardiothoracic procedures [24], and cell injection systems [25]. Wagner *et al.* [20], for example, examined the effect of haptic force feedback on a blunt dissection task and showed that system performance improved up to 150% in comparison with providing no force feedback, while also decreasing the number of tissue damaging errors by over a factor of 3. Pacchierotti *et al.* presented preliminary results of a needle steering system that provides the operator with only vibratory feedback [26]. Experiments were performed using a limited number of subjects and no path planning was implemented for obstacle avoidance. Other studies have linked the lack of significant haptic feedback to increased intraoperative injury in minimally invasive surgery operations [27] and endoscopic surgical operations [28]. Moreover, haptic feedback can prevent undesirable trauma and incidental tissue damage, as it relays surgical tool-tissue interaction forces to the operator.

Haptic feedback can be also employed to *augment* the operating environment, providing additional valuable information to the operator, such as navigation cues. For example, Nakao

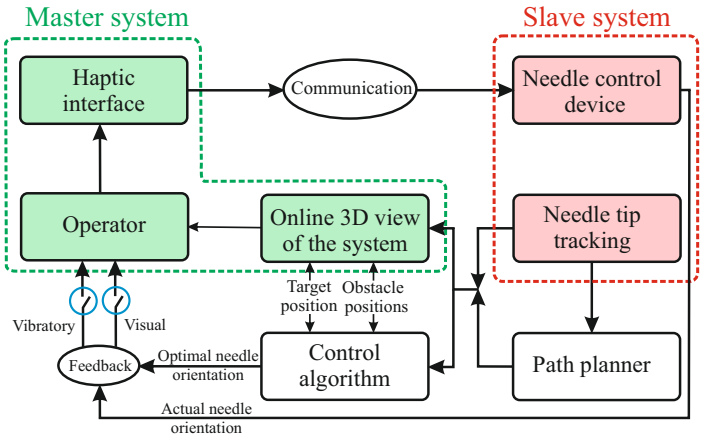

Fig. 2. Through the Omega 6 haptic device, the operator controls the motion of the slave robot and, thus, the needle. The needle tracking system provides the control algorithm and path planner with the needle tip pose. An online three-dimensional (3D) view of the needle path, position and orientation, together with the target and obstacles positions, is displayed to the operator on a computer screen. The control algorithm computes the optimal needle orientation to allow the needle to move along the planned path. The difference between the actual and the optimal needle orientations is provided to the operator with visual or vibratory feedback. The feedback system loops every 40 ms, and the planned path is updated every second.

et al. [29] presented a haptic navigation method that allows operator to avoid collision with forbidden regions during surgery. It employs kinesthetic feedback through a 2D master manipulator. More recently, Ren *et al.* [30] implemented dynamic 3D virtual constraints with haptic and visual feedback during minimally invasive beating-heart procedures.

In addition to these approaches, which mostly involve kinesthetic force feedback, there is also a growing interest in *vibratory* feedback. Van Erp *et al.* [31], for instance, employed a vibrating waist belt to provide navigation information to the operator. Results indicated the usefulness of vibratory cues for navigation purposes as well as for situational awareness in multi-tasks environments. Lieberman *et al.* [32] presented a robotic suit for improved human motor learning. It provided vibratory feedback proportional to the error between the effective and learned motion. Schoonmaker and Cao [33] demonstrated that vibratory stimulation is a viable substitute for force feedback in minimally invasive surgery, enhancing operators' ability to control the forces applied to the tissue and differentiate its softness in a simulated tissue probing task. More recently, McMahan *et al.* [34] developed a sensing and actuating device for the da Vinci S Surgical System able to provide vibrotactile feedback of tool contact accelerations. Eleven surgeons tested the system and expressed a significant preference for the inclusion of vibratory feedback.

B. Contributions

In this study, we combine the advantages of manual steering with the high accuracy of autonomous (robotic) needle insertion. The proposed system enables operators to directly control the insertion procedure while receiving navigation feedback from the control algorithm. In previous studies, visual and vibratory feedback were used only for avoiding collision or sensing tissue stiffness. To the best of our knowledge

this is the first study to use vibratory and visual feedback to give the operator navigation cues using an ultrasound-guided system with an intraoperative path planner. We carry out several experiments that allow subjects with a clinical background to control the needle orientation using different combinations of visual and vibratory feedback as computed by the control algorithm. Results are compared to the condition where the subjects control the needle orientation using only an online 3D view of the needle, target and obstacle positions, without receiving feedback from the control algorithm (Fig. 2). Different types of needle co-manipulation conditions, where the control algorithm assists the subject to steer the needle, are evaluated to achieve the highest degree of accuracy and safety. In the current study, we combine teleoperated control with path planning to steer the needle toward a target while avoiding two obstacles.

II. Materials and Methods

A. Slave System

The slave system includes the needle control device and the transducer control device. They are in charge of the needle tip tracking, control and path planning.

1) Needle Tip Tracking: Ultrasound imaging is used to track the needle tip in 3D-space during insertion. A 2D ultrasound image plane is positioned perpendicular to the insertion direction at the needle tip (see Fig. 3). The transducer moves along the needle path during insertion to keep the tip in its field-of-view. It uses a closed loop control system based on a proportional-derivative algorithm that minimizes the error between the transducer scanning velocity and the needle insertion velocity, which is obtained from the slave robot's controller. Furthermore, a Kalman observer is implemented to minimize the influence of noise on the states of location and velocity of the needle tip and to predict subsequent states according to the needle tip velocity [35].

Finally, basic image processing techniques, such as median blur, thresholding, erosion and dilation are applied on ultrasound images intra-operatively. This increases the contrast between the tip and the surrounding phantom, preventing false tip detections. After that, the system computes the needle centroid location using image moments. The controller provides an accuracy in estimating the needle tip pose up to 0.64 mm and 2.68° for position and orientation, respectively. Further details on the tracking algorithm have been presented by Vrooijink *et al.* [36].

2) Path Planning and Control Algorithms: We use a 3D path planning algorithm generate a trajectory for the needle to reach a target while avoiding obstacles in a 3D environment [37]. Using the information obtained from ultrasound images, the system provides the subjects with navigation cues to steer the needle along the planned path using the control algorithm. The needle path is planned using a customized version of the rapidly-exploring random tree (RRT) algorithm, which is a sampling-based method for path planning [38]. To enable fast performance, our path planner effectively utilizes the needles kinematics model and makes use of reachability-guided sampling for efficient expansion of the search tree. The planner is sufficiently fast that it can be executed in a closed-loop manner, updating the path every second to account for uncertainty in needle motion and changes in the environment. We refer the reader to Patil *et al.* for additional details on the planning algorithm [37].

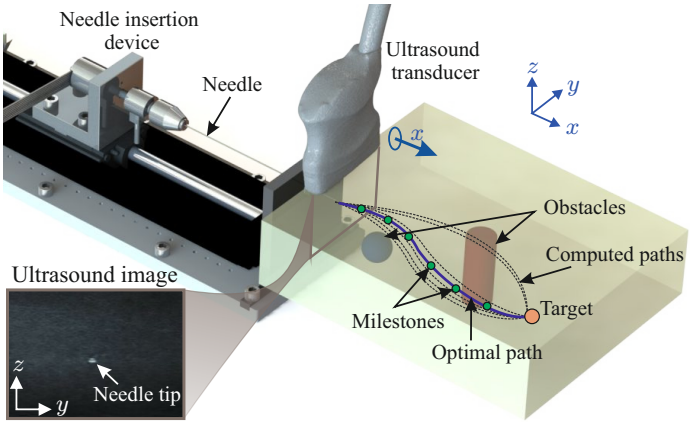

Fig. 3. The needle tip pose is determined in three-dimensional space using a two-dimensional ultrasound transducer positioned to visualize the needle tip where the ultrasound image plane is perpendicular to the needle insertion axis (x-axis). The path planning algorithm generates a feasible path by exploring the state space using a rapidly exploring random tree. The path planner generates milestones along the path, and the control algorithm steers the needle using the milestone to move along the planned trajectory.

Given pre-operative medical images, the operator can specify the insertion location, the target location, and the geometry of obstacles, which can include sensitive structures such as glands or blood vessels as well as impenetrable structures such as bones. After specifying the entire environment, the path planner computes a path that (1) reaches the target, and (2) is feasible, i.e., it avoids obstacles. The output of the path planning algorithm is a sequence of milestones along the path. The control algorithm computes the optimal orientation that allows the subject to steer the needle toward the first milestone. As soon as a milestone is reached, the control algorithm computes the optimal orientation to steer the needle toward the next milestone along the path.

The needle tip pose (position and orientation) obtained from the tracking algorithm is the main input of the control algorithm. First, the control algorithm estimates the region that the needle tip can reach during insertion. The controller then computes intra-operatively the needle tip optimal orientation every 40 ms to follow the planned trajectory and reach the target. As mentioned before, the needle can be assumed to move along arcs during its insertion into a soft-tissue phantom [5]. The direction of each arc depends on the bevel tip orientation, which is controlled by rotating the needle about its insertion axis (Fig. 3). Additional details about the control algorithm can be found in the work of Abayazid *et al.* [8], [10].

B. Master System

The master system is responsible for both steering the slave robot and displaying navigation cues regarding the optimal needle orientation. Navigation cues allows co-manipulation

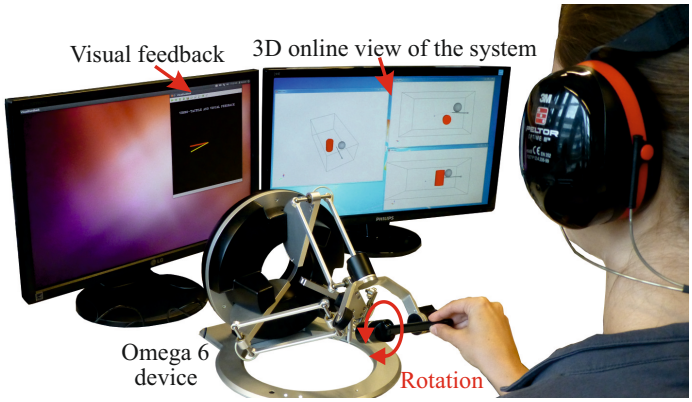

Fig. 4. Experimental evaluation. The subject performs an experimental trial while receiving both visual and vibratory feedback (VI+VB). The subject is asked to follow the online three-dimensional (3D) view of the system on the right screen and the visual feedback on the left screen.

between the subject (operator) and robotic system for needle steering. In order to avoid confusion and consequent possible errors in the medical intervention, the meaning of such cues must be easy to understand.

In this study, we propose to provide the subject with (1) an online 3D system view that includes the needle path, needle tip location, obstacle locations and target location, and (2) visual and vibratory feedback about the optimal orientation of the needle as evaluated by the control algorithm described in Sec. II-A. Details on how visual and vibratory feedback are provided to the subject are reported in Sec. II-B2 and Sec. II-B3, respectively.

1) Setup: The master system consists of two computer screens and a single-contact grounded haptic interface Omega 6 (Force Dimension, Nyon, Switzerland), as shown in Figs. 1 and 4. It provides the subject with navigation cues through visual and/or vibratory feedback, according to the feedback condition being considered (see Sec. II-C). The haptic interface allows the subject to control the orientation of the needle. In fact, the orientation of the pen-shaped haptic probe is directly linked to the orientation of the needle.

2) Visual Feedback: Two straight line segments, one red and one yellow, are presented to the subject on a computer screen (see Fig. 4). The position of one of the end points of the lines is fixed, while the other one moves on a circumference whose center is the fixed end point and whose radius is the length of the segments. The coordinates of the moving end points with respect to the center of the circumference are $(\cos\theta_i, \sin\theta_i)$ and $(\cos\theta, \sin\theta)$ for the red and yellow line, respectively, where angles $\theta_i(t)$ and $\theta(t)$ are the optimal and current orientation of the needle, respectively. The red and yellow lines thus represent the optimal and current orientation of the needle, respectively. The subject is asked to align the yellow line with the red one, since a perfect alignment of the lines denotes the least error.

3) Vibratory Feedback: Vibratory feedback is controlled by a penalty function based on the difference between the optimal orientation $\theta_i(t)$ and the current orientation $\theta(t)$ of the needle:

$$\mathbf{f_v} = \mathbf{A_1}\ |\theta_i(t) - \theta(t)|\ \ \mathrm{sgn}(\sin(\omega t)), \qquad (1)$$

where $\mathbf{A_1} = \frac{3}{\pi}\,\mathbf{I_{3\times 1}}$ N/rad and

$$\omega = \begin{cases} 100 \text{ Hz} & \text{if } \theta(t) - \theta_i(t) \geq 0, \\ 25 \text{ Hz} & \text{if } \theta(t) - \theta_i(t) < 0. \end{cases}$$

Vibrations thus provide information about the optimal orientation $\theta_i(t)$, indicating in which direction and how much the subject should rotate the pen-shaped haptic probe. Frequency ω indicates in which direction the subject should rotate the pen-shaped haptic probe: clockwise for $\omega = 100$ Hz and counter-clockwise for $\omega = 25$ Hz. Frequency values are chosen to maximally stimulate the Pacinian corpuscle receptors [39], be easy to distinguish [40] and fit the master device specifications. On the other hand, the amplitude of these vibrations indicates how much the subject should rotate the haptic probe: no vibrations indicated the best performance. Amplitude scaling matrix $\mathbf{A_1}$ is chosen to maximize the just-noticeable difference [41] for the error $|\theta_i(t) - \theta(t)|$ and fit the master device specifications.

C. Experiments

The aim of the experiments is to investigate the co-manipulation configurations that achieve sufficient targeting accuracy. We attempt to combine the advantages of a manual insertion with the high accuracy of autonomous (robotic) needle insertion.

1) Experimental protocol: The experimental setup is shown in Fig. 4. A 3D view of the planned path, target location, needle and obstacle positions using an isometric, top and side views is always displayed to the subject (right screen in Fig. 4). The task consists of rotating the pen-shape haptic probe about its axis to steer the needle toward the target point while avoiding two obstacles. The needle insertion velocity is fixed to 1 mm/s and the target point is placed at 85 mm from the insertion point. We used a Nitinol needle of 0.5 mm diameter and 30° bevel angle.

In the first three conditions, subjects receive visual and vibratory feedback from the control algorithm, in addition to the online 3D system view. In the last condition, subjects control the needle orientation relying only on the online 3D system view. Each subject made twelve randomized trials of the needle steering task, with three repetitions for each feedback condition proposed:

- visual feedback (VI) on the optimal and current orientation of the needle, as described in Sec. II-B2,
- vibratory feedback (VB) on the optimal and current orientation of the needle, as described in Sec. II-B3,
- visual and vibratory feedback (VI+VB) on the optimal and current orientation of the needle, as described in Sec. II-B2 and II-B3,
- no feedback (N) from the control algorithm on the optimal and current orientation of the needle.

2) Subjects: In order to determine the number of subjects needed for our research study, we run a power analysis using the the open source G*Power software (University of Kiel, Germany). The completion times for each trial were compared using a repeated-measures analysis of variance (ANOVA).

Table I
THE TARGETING ERROR IS CALCULATED AS THE ABSOLUTE DISTANCE BETWEEN THE NEEDLE TIP AT THE END OF INSERTION AND THE CENTER OF THE LOCALIZED TARGET. ITS MEAN ERROR IS μ AND ITS STANDARD DEVIATION IS σ. THE SUBJECT RECEIVES VISUAL (VI), VIBRATORY (VB), VISUAL AND VIBRATORY (VI+VB), OR NO (N) FEEDBACK FROM THE CONTROL ALGORITHM.

	VI	VB	VI+VB	N
μ (mm)	1.07	1.39	1.03	9.23
σ (mm)	0.59	0.70	0.64	6.68

Power analysis revealed that, in order to have a 90% chance of detecting differences in our data, we need at least 14 participants (partial $\eta^2 = 0.278$, effect size 0.621, actual power 0.918).

Fourteen subjects with medical background participated in the experiment (3 males, 11 females, age 24 - 32). The subjects participated on a voluntary basis and signed an informed consent form. Subjects were informed about the procedure before the beginning of the experiment and a 5-minute familiarization period was provided to make them acquainted with the experimental setup. Subjects were asked to wear a pair of noise canceling headphones, and they did not have direct visual access to the needle control device (slave system) in order to prevent visual cues that might alter their judgment. Before each trial, subjects were informed about which experimental condition was going to be considered.

III. RESULTS

In order to evaluate the performance of the considered feedback conditions, we evaluate the mean error in reaching the target point e_t, the mean error over time in following the optimal orientation signals e_o, and the completion time t_c. Error e_t is calculated as $\|\mathbf{n_f} - \mathbf{o_t}\|$, where $\mathbf{n_f} \in \Re^{3x1}$ represents needle tip position at the end of the task (see Table I). Errors on the optimal orientation signals e_o is computed as the mean over time of $\|\theta(t) - \theta_i(t)\|$. Data resulting from different repetitions of the same condition, performed by the same subject, were averaged before comparison with other conditions' data. Data have been transformed when necessary to meet the test's assumptions [42].

Fig. 5a shows targeting error e_t for the four experimental conditions. The collected data passed the Shapiro-Wilk normality test. Mauchly's Test of Sphericity indicated that the assumption of sphericity had been violated ($\chi^2(2) = 105.054, p < 0.001$). A repeated-measure ANOVA with a Greenhouse-Geisser correction showed a statistically significant difference between the means of the feedback conditions ($F_{1.017,13.226} = 69.734$, $p < 0.001$, a = 0.05). Post-hoc analysis (Games-Howell post-hoc test) revealed statistically significant difference between all the groups ($p < 0.001$). This means that conditions VI+VB and N performed, respectively, significantly better and worse than all the others. Condition VI outperformed condition VB.

Fig. 5b shows orientation error e_o for the four experimental conditions. The collected data passed the Shapiro-Wilk normality test. Mauchly's Test of Sphericity indicated that the assumption of sphericity had been violated ($\chi^2(2) = 12.843, p = 0.025$). A repeated-measure ANOVA with a Greenhouse-Geisser correction showed a statistically significant difference between the means of the feedback conditions ($F_{1.741,22.628} = 83.849$, $p < 0.001$, a = 0.05). Post-hoc analysis (Games-Howell post-hoc test) revealed statistically significant difference between all the groups (VI vs VB, $p = 0.016$; VI vs VI+VB, $p = 0.035$; VI vs N, $p < 0.001$; VB vs VI+VB, $p < 0.001$; VB vs N, $p < 0.001$; VI+VB vs N, $p < 0.001$). As for Fig. 5a, this also means that conditions VI+VB and N performed, respectively, significantly better and worse than all the others. Condition VI outperformed condition VB.

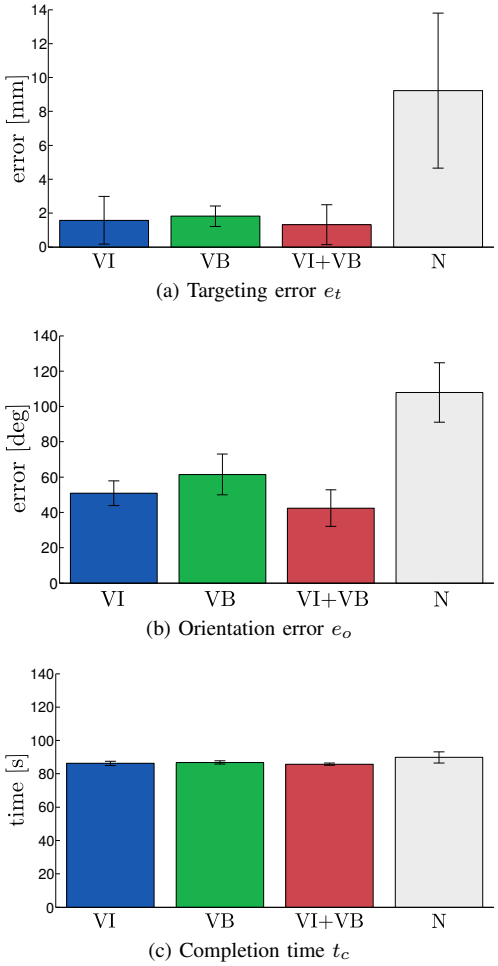

(a) Targeting error e_t

(b) Orientation error e_o

(c) Completion time t_c

Fig. 5. Needle insertion experiment. Targeting error e_t, orientation error e_o, and completion time t_c (mean and SD) are plotted for the experimental conditions where the subjects receive visual (VI), vibratory (VB), visual and vibratory (VI+VB), and no (N) feedback from the control algorithm. Lower values of this metrics indicate higher performances in completing the given task.

Fig. 5c shows the completion time t_c for the four experimental conditions. The collected data passed the Shapiro-Wilk normality test. Mauchly's Test of Sphericity indicated that the assumption of sphericity had been violated ($\chi^2(2) = 24.629, p < 0.001$). A repeated-measure ANOVA with a Greenhouse-Geisser correction showed a statistically significant difference between the means of the feedback conditions ($F_{1.380,17.942} = 16.440$, $p < 0.001$, a = 0.05). Post-hoc analysis (Games-Howell post-hoc test) revealed statistically significant difference between conditions N and all the others (VI vs N,

Table II
SUBJECTS' EXPERIENCE EVALUATION. PARTICIPANTS RATED THESE STATEMENTS, PRESENTED IN RANDOM ORDER, USING A 7-POINT LIKERT SCALE (1 = COMPLETELY DISAGREE, 7 = COMPLETELY AGREE). MEANS AND STANDARD DEVIATIONS ARE REPORTED FOR THE VISUAL (VI), VIBRATORY (VB), VISUAL-VIBRATORY (VI+VB), AND NO FEEDBACK (VI) CONDITIONS.

		Questions	**Mean**	σ
General	Q1	The system was intuitive.	3.36	1.08
	Q2	The system was easy to use.	3.79	0.70
	Q3	I needed support by the test administrator to be able to use the system.	2.50	1.16
	Q4	Most people would quickly learn how to use the system.	3.57	0.94
	Q5	I felt confident using the system.	3.00	1.11
	Q6	I needed more training to confidently use the system.	3.43	1.40
	Q7	Sound from the device caused disturbance while performing the experiments.	1.71	0.99
	Q8	I was well-isolated from external noises.	3.86	1.51
	Q9	At the end of the experiment I felt tired.	2.36	1.01
	Q10	I found useful to see the 3D representation of the needle insertion.	3.71	0.91
VI	Q11	In this feedback condition I performed the best.	3.76	1.12
	Q12	In this feedback condition I could pay attention to the 3D representation of the needle.	2.07	1.14
VB	Q13	In this feedback condition I performed the best.	3.29	0.99
	Q14	In this feedback condition I could pay attention to the 3D representation of the needle.	3.93	1.07
VI+VB	Q15	In this feedback condition I performed the best.	4.00	1.41
	Q16	In this feedback condition I could pay attention to the 3D representation of the needle.	2.21	1.19
N	Q17	In this feedback condition I performed the best.	1.71	1.14
	Q18	In this feedback condition I could pay attention to the 3D representation of the needle.	4.14	1.17

$p = 0.013$; VB vs N, $p = 0.015$; VI+VB vs N, $p = 0.001$), and between conditions VB and VI+VB ($p = 0.009$). This means that subjects took significantly more time to complete the task while being provided with no feedback from the controller (condition N). On the other hand, subjects complete the task significantly faster in condition VI+VB than in condition VB.

In addition to the quantitative evaluation presented above, we also measured subjects' experience. Immediately after the experiment, participants were asked to fill in a 18-item questionnaire using bipolar Likert-type seven-point scales. It contained a set of assertions, where a score of 7 was described as "completely agree" and a score of 1 as "completely disagree" with the assertion. The evaluation of each question is reported in Table II. Fig. 6 shows the mean ratings given by the subjects in eight questions of the post-experimental questionnaire. Fig. 6a shows the ratings given by the subjects to the question "In this feedback condition I performed the best" across the four different feedback conditions (Q11 vs. Q13 vs. Q15 vs. Q17, see Table II). Since the data were registered at the ordinal level, we ran a Friedman test. Ratings were statistically significantly different for different feedback conditions, $\chi^2(3) = 18.378$, $p < 0.001$. Pairwise comparisons were performed with a Bonferroni correction for multiple comparisons. Ratings were statistically significantly different between condition N and all the others (VI vs N, $p = 0.013$; VB vs N, $p = 0.032$; VI+VB vs N, $p = 0.001$). This means that subjects felt that they performed significantly worse in condition N with respect to all the others. Fig. 6b shows the ratings given to the question "In this feedback condition I could pay attention to the 3D representation of the needle" across the four feedback conditions (Q12 vs. Q14 vs. Q16 vs. Q18, see Table II). This question has been asked to evaluate the ability of the subject to monitor the overall insertion procedure using the 3D system view while performing the experiments. We ran again a Friedman test. Ratings were statistically significantly different across the feedback conditions, $\chi^2(3) = 21.095$, $p < 0.001$. Pairwise comparisons were performed with a Bonferroni correction for multiple comparisons. Ratings were statistically significantly different between conditions VI and VB ($p = 0.008$), VI and N ($p = 0.008$), VB and VI+VB ($p = 0.020$), VI+VB and N ($p = 0.020$). This shows that, as expected, providing the subjects with visual feedback about the optimal orientation of the needle prevented them from focusing on the 3D view of the system (see Fig. 4). On the other hand, conditions VB and N enabled the subjects to look at the 3D view of the system. *Please refer to the accompanying video as supplementary material that demonstrates the experimental results.*

IV. DISCUSSION

Results show that all the subjects were able to steer the needle with an accuracy of $\sim$1 mm, while receiving feedback from the control algorithm. The mean targeting accuracy improved 9 times while receiving visual, vibratory or combined feedback with respect to the condition where no navigation feedback from the control algorithm was provided to the subjects. This shows that steering of bevel-tipped needle is not trivial, and receiving an online 3D view of the system may not be sufficient for accurate steering. Moreover, the needle hit an obstacle in 9 trials (out of 42) while receiving no navigation

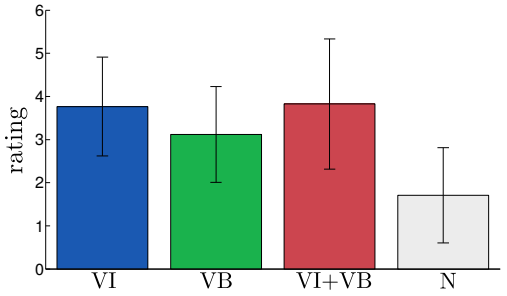

(a) In this feedback condition I performed the best. (Q11 vs. Q13 vs. Q15 vs. Q17, see Table II)

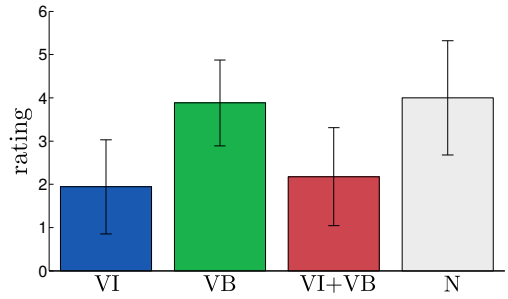

(b) In this feedback condition I could pay attention to the 3D representation of the needle. (Q12 vs. Q14 vs. Q16 vs. Q18, see Table II)

Fig. 6. Questionnaire. Answers (mean and SD) are plotted for the experimental conditions where the subjects receive visual (VI), vibratory (VB), visual and vibratory (VI+VB), and no (N) feedback from the control algorithm.

feedback from the control algorithm (N), while the collision never occurred while receiving any type of control feedback (VI, VB, or VI+VB).

According to our post-experiment questionnaire, subjects preferred visual feedback (VI) over vibratory feedback (VB). The reason can be that humans are more used to deal with visual cues with respect to vibratory ones, and, therefore, they feel more comfortable with them. However, employing visual feedback did not give the subject the chance to follow the 3D system view. It was difficult for the subject to follow the online 3D system view (to monitor the overall insertion procedure) while receiving visual feedback from the control algorithm about the optimal and current orientation of the needle (VI and VI+VB) (Fig. 4).

A. Conclusions

In this study, we present a teleoperation system to steer bevel-tipped flexible needles. An ultrasound-guided system with an intraoperative path planner is used to assist the subject to steer the needle tip toward a target while avoiding two obstacles. The system enables subjects to directly maneuver the surgical tool while providing them with navigation cues through visual and vibratory feedback. Fully autonomous medical robotic systems are still not totally accepted by the medical community due to safety reasons. For this reason, in our work, a control algorithm computes the optimal needle orientation during insertion but the needle motion is directly controlled by the subject. The optimal orientation is provided to the master interface, which presents it to the subject, who commands the slave robot and steers the needle to follow the planned path. Four experimental conditions are taken into account. Subjects control the needle orientation using visual, vibratory, visual and vibratory (combined) or no feedback from the control algorithm. In all conditions subjects are provided with an online 3D view of the needle, target and obstacle positions. A questionnaire is also filled in by the subjects to obtain feedback about their experience with different co-manipulation configurations.

Experimental results show that navigation cues provided by the control algorithm (VI, VB and VI+VB) improve the targeting accuracy with respect to the experimental condition where only the online 3D view is displayed (N) for the subject. This result confirms the hypothesis that bevel-tipped needles are difficult to be manually steered without feedback. Although the targeting accuracy is similar for the three conditions with feedback from the control algorithm, the subjects felt more comfortable receiving visual feedback. However, they conclude that using vibratory feedback is convenient since it enables them to monitor the needle trajectory during the insertion.

B. Future Work

We will estimate the needle behavior during insertion in different biological tissues. Advanced image processing algorithms should be implemented to track the needle tip in biological tissue. The steering system can also be extended to detect the patient movements that occur during needle insertion such as respiration and fluid flow. Finally, work is in progress to use kinesthetic force to provide subjects with force feedback regarding the mechanical properties of the tissue being penetrated.

Acknowledgments

The authors would like to thank Sachin Patil for his earlier contributions in developing the path planning algorithm.

Funding

The research leading to these results has received funding from the Netherlands Organization for Scientific Research (NWO-Project: 11204) and from the European Union Seventh Framework Programme FP7/2007-2013 under grant agreement n° 270460 of the project “ACTIVE - Active Constraints Technologies for Ill-defined or Volatile Environments” and under grant agreement n° 601165 of the project “WEARHAP - WEARable HAPtics for humans and robots”. This research was also supported in part by the United States National Science Foundation (NSF) through award IIS-1149965 and by the United States National Institutes of Health (NIH) under award R21EB011628.

Conflict of Interest

The authors have declared that there is no conflict of interest.

References

[1] E. M. Boctor, M. A. Choti, E. C. Burdette, and R. J. Webster III, “Three-dimensional ultrasound-guided robotic needle placement: an experimental evaluation,” *The International Journal of Medical Robotics and Computer Assisted Surgery*, vol. 4, no. 2, pp. 180–191, 2008.

[2] P. Beddy, R. D. Rangarajan, and E. Sala, "Role of MRI in intracavitary brachytherapy for cervical cancer: What the radiologist needs to know," *American Journal of Roentgenology*, vol. 196, no. 3, pp. W341–W347, 2011.

[3] R. Seifabadi, S.-E. Song, A. Krieger, N. Cho, J. Tokuda, G. Fichtinger, and I. Iordachita, "Robotic system for mri-guided prostate biopsy: feasibility of teleoperated needle insertion and ex vivo phantom study," *International Journal of Computer Assisted Radiology and Surgery*, vol. 7, no. 2, pp. 181–190, 2012.

[4] N. J. Cowan, K. Goldberg, G. S. Chirikjian, G. Fichtinger, K. B. Reed, V. Kallem, W. Park, S. Misra, and A. M. Okamura, *Surgical Robotics*, ch. Robotic Needle Steering: Design, Modeling, Planning, and Image Guidance, pp. 557–582. Springer US, 2011.

[5] R. J. Webster, J. S. Kim, N. J. Cowan, G. S. Chirikjian, and A. M. Okamura, "Nonholonomic modeling of needle steering," *International Journal of Robotics Research*, vol. 25, no. 5-6, pp. 509–525, 2006.

[6] J. A. Engh, G. Podnar, S. Y. Khoo, and C. N. Riviere, "Flexible needle steering system for percutaneous access to deep zones of the brain," in *Proceedings of the IEEE Annual Northeast Bioengineering Conference (NEBEC)*, pp. 103–104, Easton, USA, April 2006.

[7] K. Hauser, R. Alterovitz, N. Chentanez, A. M. Okamura, and K. Goldberg, "Feedback control for steering needles through 3d deformable tissue using helical paths," in *Proceedings of Robotics: Science and Systems (RSS)*, vol. 37, Seattle, USA, June 2009.

[8] M. Abayazid, R. J. Roesthuis, R. Reilink, and S. Misra, "Integrating deflection models and image feedback for real-time flexible needle steering," *IEEE Transactions on Robotics*, vol. 29, no. 2, pp. 542–553, 2013.

[9] M. Abayazid, M. Kemp, and S. Misra, "3d flexible needle steering in soft-tissue phantoms using fiber bragg grating sensors," in *Proceedings of the IEEE International Conference on Robotics and Automation (ICRA)*, pp. 5823–5829, Karlsruhe, Germany, May 2013.

[10] M. Abayazid, G. J. Vrooijink, S. Patil, R. Alterovitz, and S. Misra, "Experimental evaluation of ultrasound-guided 3d needle steering in biological tissue," *International Journal of Computer Assisted Radiology and Surgery (IJCARS)*, pp. 1–9, 2014, DOI:10.1007/s11548-014-0987-y.

[11] J. Troccaz, M. Peshkin, and B. Davies, "Guiding systems for computer-assisted surgery: introducing synergistic devices and discussing the different approaches," *Medical Image Analysis*, vol. 2, no. 2, pp. 101–119, 1998.

[12] J. M. Romano, R. J. Webster, and A. M. Okamura, "Teleoperation of steerable needles," in *Proceedings of the IEEE International Conference on Robotics and Automation (ICRA)*, pp. 934–939, Roma, Italy, April 2007.

[13] N. Hungr, J. Troccaz, N. Zemiti, and N. Tripodi, "Design of an ultrasound-guided robotic brachytherapy needle-insertion system," in *Proceedings of the IEEE international conference on Engineering in Medicine and Biology Society (EMBC)*, pp. 250–253, Minneapolis, MN, USA, September 2009.

[14] A. Majewicz and A. M. Okamura, "Cartesian and joint space teleoperation for nonholonomic steerable needles," in *World Haptics Conference (WHC)*, pp. 395–400, Daejeon, Korea, April 2013.

[15] M. G. Schouten, J. Ansems, W. K. J. Renema, D. Bosboom, T. W. J. Scheenen, and J. J. Fütterer, "The accuracy and safety aspects of a novel robotic needle guide manipulator to perform transrectal prostate biopsies," *Medical Physics*, vol. 37, pp. 4744–4750, September 2010.

[16] D. Yakar, M. G. Schouten, D. G. H. Bosboom, J. O. Barentsz, T. W. J. Scheenen, and J. J. Ftterer, "Feasibility of a pneumatically actuated mr-compatible robot for transrectal prostate biopsy guidance," *Radiology*, vol. 260, pp. 241–247, January 2011.

[17] D. Prattichizzo, C. Pacchierotti, and G. Rosati, "Cutaneous force feedback as a sensory subtraction technique in haptics," *IEEE Transactions on Haptics*, vol. 5, no. 4, pp. 289–300, 2012.

[18] L. Meli, C. Pacchierotti, and D. Prattichizzo, "Sensory subtraction in robot-assisted surgery: fingertip skin deformation feedback to ensure safety and improve transparency in bimanual haptic interaction," *IEEE Transactions on Biomedical Engineering*, vol. 61, no. 4, pp. 1318–1327, 2014.

[19] C. Pacchierotti, A. Tirmizi, and D. Prattichizzo, "Improving transparency in teleoperation by means of cutaneous tactile force feedback," *ACM Transactions on Applied Perception (TAP)*, vol. 11, no. 1, pp. 4:1–4:16, 2014.

[20] C. R. Wagner, N. Stylopoulos, and R. D. Howe, "The role of force feedback in surgery: analysis of blunt dissection," in *Proceedings of the Symposium of Haptic Interfaces for Virtual Environment and Teleoperator Systems*, pp. 68–74, 2002.

[21] S. E. Salcudean, S. Ku, and G. Bell, "Performance measurement in scaled teleoperation for microsurgery," in *Proceedings of the First Joint Conference on Computer Vision, Virtual Reality and Robotics in Medicine and Medial Robotics and Computer-Assisted Surgery*, pp. 789–798, Grenoble, France, 1997.

[22] A. Kazi, "Operator performance in surgical telemanipulation," *Presence: Teleoperators & Virtual Environments*, vol. 10, no. 5, pp. 495–510, 2001.

[23] L. Moody, C. Baber, T. N. Arvanitis, *et al.*, "Objective surgical performance evaluation based on haptic feedback," *Studies in health technology and informatics*, vol. 85, pp. 304–310, 2002.

[24] C. W. Kennedy, T. Hu, J. P. Desai, A. S. Wechsler, and J. Y. Kresh, "A novel approach to robotic cardiac surgery using haptics and vision," *Cardiovascular Engineering*, vol. 2, no. 1, pp. 15–22, 2002.

[25] A. Pillarisetti, M. Pekarev, A. D. Brooks, and J. P. Desai, "Evaluating the effect of force feedback in cell injection," *IEEE Transactions on Automation Science and Engineering*, vol. 4, no. 3, pp. 322–331, 2007.

[26] C. Pacchierotti, M. Abayazid, S. Misra, and D. Prattichizzo, "Steering of flexible needles combining kinesthetic and vibratory force feedback," in *Proceeding of the IEEE Conference on Intelligent Robots and Systems (IROS)*, pp. 1202–1207, Chicago, USA, September 2014.

[27] A. M. Okamura, "Haptic feedback in robot-assisted minimally invasive surgery," *Current opinion in urology*, vol. 19, no. 1, pp. 102–107, 2009.

[28] M. Hashizume, M. Shimada, M. Tomikawa, Y. Ikeda, I. Takahashi, R. Abe, F. Koga, N. Gotoh, K. Konishi, S. Maehara, *et al.*, "Early experiences of endoscopic procedures in general surgery assisted by a computer-enhanced surgical system," *Surgical endoscopy*, vol. 16, no. 8, pp. 1187–1191, 2002.

[29] M. Nakao, K. Imanishi, T. Kuroda, and H. Oyama, "Practical haptic navigation with clickable 3d region input interface for supporting master-slave type robotic surgery," *Studies in Health Technology and Informatics*, pp. 265–271, 2004.

[30] J. Ren, R. V. Patel, K. A. McIsaac, G. Guiraudon, and T. M. Peters, "Dynamic 3-d virtual fixtures for minimally invasive beating heart procedures," *IEEE Transactions on Medical Imaging*, vol. 27, no. 8, pp. 1061–1070, 2008.

[31] J. B. F. van Erp, H. A. H. C. van Veen, C. Jansen, and T. Dobbins, "Waypoint navigation with a vibrotactile waist belt," *ACM Transactions on Applied Perception*, vol. 2, no. 2, pp. 106–117, 2005.

[32] J. Lieberman and C. Breazeal, "Tikl: Development of a wearable vibrotactile feedback suit for improved human motor learning," *IEEE Transactions on Robotics*, vol. 23, no. 5, pp. 919–926, 2007.

[33] R. E. Schoonmaker and C. G. L. Cao, "Vibrotactile feedback enhances force perception in minimally invasive surgery," in *Proc. of Human Factors and Ergonomics Society Annual Meeting*, vol. 50, pp. 1029–1033, 2006.

[34] W. McMahan, J. Gewirtz, D. Standish, P. Martin, J. A. Kunkel, M. Lilavois, A. Wedmid, D. I. Lee, and K. J. Kuchenbecker, "Tool contact acceleration feedback for telerobotic surgery," *IEEE Transactions on Haptics*, vol. 4, no. 3, pp. 210–220, 2011.

[35] Y. Bar-Shalom, X. R. Li, and T. Kirubarajan, *Estimation with Applications to Tracking and Navigation: Theory Algorithms and Software*. John Wiley and Sons, Inc., July 2001.

[36] G. J. Vrooijink, M. Abayazid, S. Patil, R. Alterovitz, and S. Misra, "Needle path planning and steering in a three-dimensional non-static environment using two-dimensional ultrasound images," *International Journal of Robotics Research*, vol. 33, pp. 1361–1374, June 2014.

[37] S. Patil and R. Alterovitz, "Interactive motion planning for steerable needles in 3d environments with obstacles," in *Proceedings of IEEE RAS and EMBS International Conference on Biomedical Robotics and Biomechatronics (BioRob)*, pp. 893–899, Tokyo, Japan, September 2010.

[38] S. M. LaValle, *Planning Algorithms*. Cambridge University Press, 2006.

[39] R. W. Cholewiak and A. A. Collins, "Sensory and physiological bases of touch," in *The Psychology of Touch* (M. A. Heller and W. Schiff, eds.), pp. 13–60, Laurence Erlbaum Associates, 1991.

[40] K. A. Kaczmarek, J. G. Webster, P. Bach-y Rita, and W. J. Tompkins, "Electrotactile and vibrotactile displays for sensory substitution systems," *IEEE Transactions on Biomedical Engineering*, vol. 38, no. 1, pp. 1–16, 1991.

[41] H. Pongrac, "Vibrotactile perception: examining the coding of vibrations and the just noticeable difference under various conditions," *Multimedia systems*, vol. 13, no. 4, pp. 297–307, 2008.

[42] S. Wallenstein, C. L. Zucker, and J. L. Fleiss, "Some statistical methods useful in circulation research," *Circulation Research*, vol. 47, no. 1, pp. 1–9, 1980.